

AD-A103 691 FOREIGN TECHNOLOGY DIV WRIGHT-PATTERSON AFB OH
JOURNAL OF ENGINEERING THERMOPHYSICS (SELECTED ARTICLES), (U)
AUG 81 H SHEN, Z CHEN, D WU, Z YANG, R ZHANG
UNCLASSIFIED FTD-ID(RS)T-0552-81

F/G 20/4

NL

| C9 |
AC
AD-SEM

B

10-81

END
DATE
10-81
DTIC

ADA103691

FTD-ID(RS)T-0552-81 ✓
BS

FOREIGN TECHNOLOGY DIVISION



JOURNAL OF ENGINEERING THERMOPHYSICS
(Selected Articles)

81 9 02 053



DTIC
ELECTED
SEP 3 1981
S D
D

Approved for public release;
distribution unlimited.



Accession For	
NTIS GRA&I	X
DTIC TAB	
Unannounced	
Justification	
By	
Distribution/	
Availability Codes	
Avail and/or	
Dist Special	
A	

FTD-ID(RS)T-0552-81

EDITED TRANSLATION

14) FTD-ID(RS)T-0552-81

11) 7 August 1981

MICROFICHE NR: FTD-81-C-000727

① JOURNAL OF ENGINEERING THERMOPHYSICS
Selected Articles) ② ③ ④ ⑤ ⑥

English pages: 52

Source: Journal of Engineering Thermophysics,
Vol. 1, Nr. 3, August 1980,
pp. 237-254, 265-272

Country of origin: (China)

Translated by: SCITRAN
F33657-78-D-0619

Requester: FTD/TQTA

Approved for public release; distribution
unlimited.

Hui-li / Shen Zhong-qing / Chen
Da / Wu Zai-ming / Yang Rung / Zhang

THIS TRANSLATION IS A RENDITION OF THE ORIGINAL FOREIGN TEXT WITHOUT ANY ANALYTICAL OR EDITORIAL COMMENT. STATEMENTS OR THEORIES ADVOCATED OR IMPLIED ARE THOSE OF THE SOURCE AND DO NOT NECESSARILY REFLECT THE POSITION OR OPINION OF THE FOREIGN TECHNOLOGY DIVISION.

PREPARED BY:

TRANSLATION DIVISION
FOREIGN TECHNOLOGY DIVISION
WP-AFB, OHIO.

FTD-ID(RS)T-0552-81

Date 7 Aug 1981

141600

JOB

TABLE OF CONTENTS

Analytical and Experimental Investigation of Performance of Supersonic Ejector Nozzle, by <u>Shen Hui-li</u> and <u>Chen</u> <u>Zhong-qing</u>	1
Analytical and Experimental Investigation of Supersonic Ejector Nozzle, by <u>Wu Da</u> , <u>Yang Zai-ming</u> and <u>Zhang Rung</u>	18
B ₁ Type Transonic Axial-Flow-Compressor First Stage Rotor Blade Design, Test and Application, by Zhou Wei-guo.....	37

ANALYTICAL AND EXPERIMENTAL INVESTIGATION OF PERFORMANCE
OF SUPERSONIC EJECTOR NOZZLE*

Shen Hui-li and Chen Zhong-qing
(Northwestern Polytechnical University)

SUMMARY

This article introduces a theoretical method of calculation for the flow field and performance of a supersonic ejector nozzle. It includes such calculations as those listed here, that is, the real sonic line at the exit of the primary jet nozzle, the non-viscid flow flow field, the adjustments for the influence of viscosity, pumping performance and thrust performance.

In order to make the results of calculations agree even better with the data obtained from experiments, one can employ the real sonic line and not the planar sonic line as the initial base line for calculations. The real sonic line is obtained from the points of intersection between the constant flow angle lines in the throat region of the primary jet nozzle and the Mach lines which occur in the lip region of the primary jet nozzle. First, one needs to calculate the non-viscid flow flow field of the primary jet nozzle and then, after that is done, make adjustments taking into consideration the effects of viscosity. The method which is employed in this article for adjustment to correct for the effects of viscosity consists of replacing the original geometric coordinates of the ejector shroud with the corrected geometrical coordinates for the shroud. The former are obtained by taking the displacement thicknesses for the mixed region and the boundary layers and superimposing them on the original geometrical coordinates for the shroud. Calculations of the actual flow field of the jet nozzle and the pumping performance as

* This article was read at the 2nd Annual All-China Thermophysical Engineering Technology Conference in Hangzhou in November 1978.

well as other related quantities are done on the basis of the corrected coordinates. The method for making these corrections is relatively simple and adequately accurate.

These calculations were done on a "320" digital computer and model testing was done at a ground facility. The theoretical and actual results are in basic agreement.

ILLUSTRATIONS OF FLOW FORMS [1,2]

1. High harmonic flows (Figure 1). When the amount of flow involved in harmonic flows is small, the main flow, after it flows out of the main jet nozzle, continues to increase its acceleration in the expansion section of the "flow body wall surface". The harmonic flow involved accelerates in the passage formed by the surface of the shroud and the "flow body wall surface". Depending on the dimensions of the ejector nozzle involved and the conditions of the flow being considered, there are three types of possible situations. These are the maintaining of subsonic speed in the harmonic flow, the existence of sonic speeds at the end surface of the jet nozzle within the harmonic flow, and the existence of supersonic speeds in the harmonic flow on the end surface of the jet nozzle. Because of the effects of the viscosity of the gases involved, there is formed in the interval between the main flow and the harmonic flow a non-isobaric mixed region and there is also formed a boundary layer on the wall surface of the shroud. However, in the case in which one is dealing with a high harmonic flow, the influence of viscosity is relatively small.

2. Low harmonic flows (Figure 2). When the quantity of flow involved in a situation is relatively small (or approaches zero), then the main flow takes the form of a free jet and expands into an isobaric area. This jet adheres to the wall surface of the expansion section of the harmonic flow and, going through a violent recompression, forms a shock wave. In the upper reaches of this section,

there is formed a dead zone by the low speed isobaric gas body which is adjacent to the boundaries of the isobaric area. Along the boundaries of the main flow, due to the effects of the viscosity of the gases, there is also a mixed region which separates the main flow from the dead zone. Inside this mixed region, there is an exchange of mass and energy between the main flow and the harmonic flows. Due to the effects of viscosity, the main flow continuously pulls out a certain amount of the harmonic flow from the dead zone, and this section of the harmonic flow which is pulled away is then replaced by the harmonic flow gas supply system.

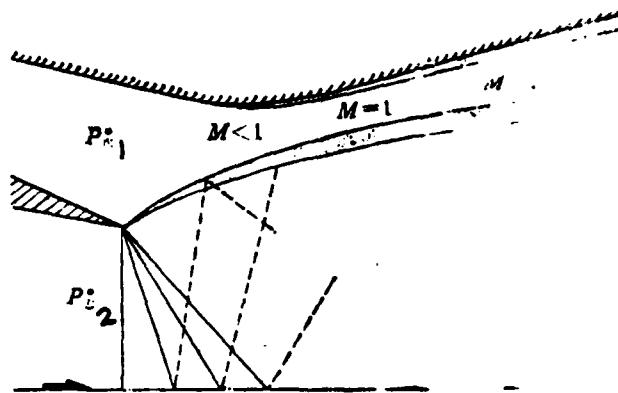


Figure 1. An illustration of the flow in the high harmonic flow within an ejector nozzle.

1--harmonic; 2--main

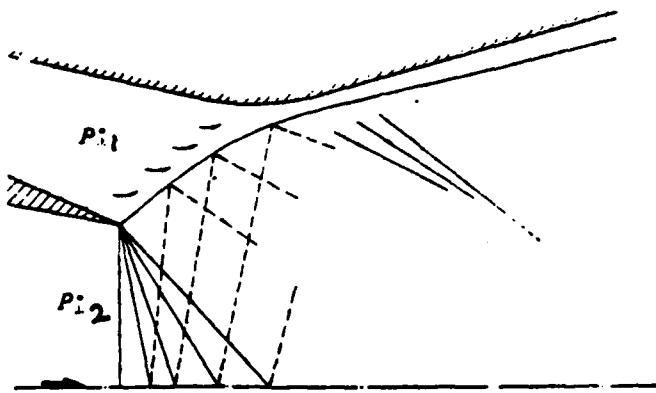


Figure 2. An illustration of the flow in the low harmonic flow inside an ejector nozzle
1--harmonic; 2--main

CALCULATION METHODS

1. The calculation of the real sonic line [3]. The real sonic line is determined after one determines the angle of flow of the transonic area in the throat section of the main jet nozzle and the Mach lines of the lip of the main jet nozzle (Figure 3). If we make the assumptions that the flow involved is stable, irrotational, isoentropic and two-dimensional, then this type of flow can be described by using a flow function equation, that is

$$[1 - (\rho^*/\rho)^2 \Psi_x^2/a^2] \Psi_{xx} + [2(\rho^*/\rho)^2 \Psi_x \Psi_y/a^2] \Psi_{xy} + [1 - (\rho^*/\rho)^2 \Psi_y^2/a^2] \Psi_{yy} = 0 \quad (1)$$

In this equation, the subscripts are the partial derivatives chosen for x or y . The input definition is $q = (u^2 + v^2)^{1/2}$, $\theta = \arctg(v/u)$ pertaining to the speed variable and, in such a case, Equation (1) becomes

$$\partial[(\rho^*/\rho)q(\partial\Psi/\partial q)]/\partial q + (\rho^*/\rho)(1/q)(1 - q^2/a^2)\partial^2\Psi/\partial\theta^2 = 0 \quad (2)$$

If we again use the definition $d\omega = (\rho/\rho^*)(dq/q)$ and its transformed speed, then Equation (2) can be simplified to be

$$\partial^2\Psi/\partial\omega^2 + k(M)\partial^2\Psi/\partial\theta^2 = 0 \quad (3)$$

In this equation $k(M) = (\rho^*/\rho)^2(1 - M^2)$.

If we make the "tangential gas assumption" $k(M) = 1$, on the basis of the fact that the speed graph relationships can be simplified into the form of Cauchy-Riemann equations, it is then possible to solve the flow field involved by the use of the complex variable method. Compressible and non-compressible flows are related by the equation $d\omega = (\rho/\rho^*)(dq/q)$, and after we do an integration of this, we obtain

$$\omega = \ln[2(q/q_m)(M_m/\sqrt{1 - M_m^2})/(1 + \sqrt{1 + (q/q_m)^2 M_m^2/(1 - M_m^2)})] \quad (4)$$

In this equation, q_m and M_m represent the speed parameter and M number for a matching configuration. Because of the fact that the Cauchy-Riemann conditions are satisfied, because the boundary conditions are at the boundaries being studied, it is possible to make

use of a set of original and combined complex fluctuations with the conditions

$$F(\omega - i\theta) = \ln[(\cosh \omega_1 - \cosh \omega_2)/(\cosh \omega_2 - 1)] \quad (5)$$

In this equation

$$\omega_1 = (\omega - i\theta - \omega_1) \cdot \pi/a; \quad \omega_2 = (\omega_1 - \omega_2) \cdot \pi/a$$

If we carry out a differentiation of Equation (5), then we obtain the complex speed

$$\begin{aligned} dF/d(\omega - i\theta) &= (\pi/a) \sinh \omega_1 / (\cosh \omega_2 - \cosh \omega_1) \\ &\quad - (\pi/a) \sinh \omega_2 / (\cosh \omega_2 - 1) \end{aligned} \quad (6)$$

Concerning the use of this to reach solutions in situations in which there is a finite conical jet tube, after we introduce the complex variable $z = \xi + iy$, then it becomes possible to take a graphic solution for the speed and transfer it to the physical plane. When this is done, then

$$\begin{aligned} dz &= (1/e^{\omega-i\theta}) [dF/d(\omega - i\theta)] d(\omega - i\theta) \\ &\quad - (\overline{e^{\omega-i\theta}/4}) [\overline{dF/d(\omega - i\theta)}] \overline{d(\omega - i\theta)} \end{aligned} \quad (7)$$

In this equation, the last quantity with the horizontal line represents the complex conjugate value. Concerning the integration of Equation (7), it is possible to obtain the point (x, y) in the speed plane. The numerical constant in the equation can be adjusted in this way to cause the position of the jet nozzle lip in the speed plane (ω_1, a) to correspond to the point $(0, 1)$ on the physical plane. What is particularly useful for us in this type of analysis is the distribution of the flow angles of the throat region. The line along which the angles of flow are equal is called the "constant flow angle line". In order to obtain the equation for the constant flow angle line, we carry out a numerical value integration for values of ω from ω_a to ω_1 in the range in which the flow angle lies between 0 and α .

One makes use of the characteristic curve method in calculating the Mach line for the lip of the jet nozzle. The main equations which are used in this process are set out in a following section.

In the lip section of a jet nozzle, the expansion is of a central wave type and satisfies the Prandtl-Meyer function. Concerning the fact that the flow in the lip section of the jet nozzle turns through a certain angle, the expansion process can be divided into separate finite numerical procedures. The first point on the sonic line is the point of intersection (Figure 3) of the first constant flow angle (the angle of flow is α) and the Mach line for the lip of the jet nozzle. As far as the other different points on the sonic line, they are solved for in an analogous way.

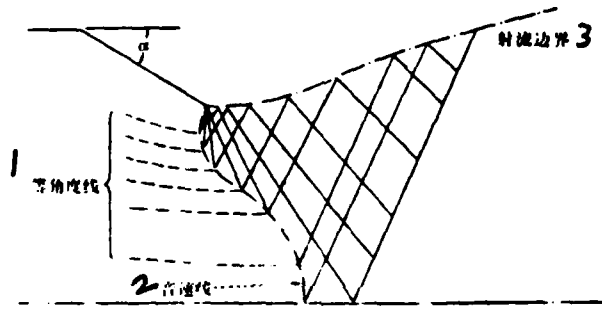


Figure 3. The real sonic line
1--constant flow angle line; 2--sonic line; 3--jet boundary

2. The calculation of the flow field of high harmonic non-viscous flow and its characteristics (Figure 4)

(1) Assume that the harmonic flow is one-dimensional and iso-entropic in its nature. Assume that the static pressures for the two sides of each point on the boundary of the harmonic and main flows are equal and further assume that the main flow is non-viscous in nature and is constrained by the characteristic curve.

(2) Concerning conditions which are already known, the initial conditions concerning the main flow include total pressure, total temperature and the amount of flow. These conditions also include the total pressure of the harmonic flow as well as its total temperature, and the external boundary atmospheric pressure. The geometrical dimensions of the ejector nozzle are also included.

(3) The principal formulae used are [6]

$$G = mdq(\lambda)p^*/\sqrt{T^*} \quad (8)$$

$$\mu = \arcsin(1/M) \quad (9)$$

$$\lambda^2 = 1 + [2/(k-1)] \sin^2 [\sqrt{(k-1)/(k+1)} \cdot \theta] \quad (10)$$

$$dy/dx = \tan(\phi \pm \mu), \quad dy/dx = \tan \phi \quad ds = 0$$

$$(\delta p/p)(\sqrt{M^2 - 1/kM^2}) + \delta \phi = -(\sin \phi / MR)\delta \eta \quad (11)$$

$$(\delta p/p)(\sqrt{M^2 - 1/kM^2}) - \delta \phi = -(\sin \phi / MR)\delta \xi \quad (12)$$

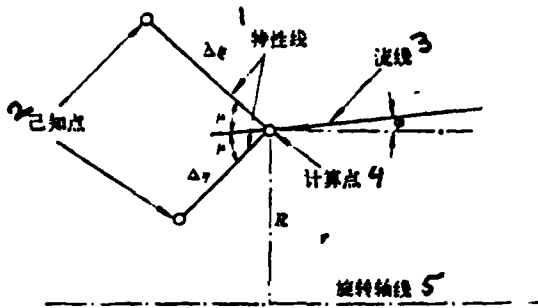


Figure 4. A computational diagram for an ejector nozzle.

1--characteristic curve; 2--an already-known point; 3--line of flow;
4--computation point; 5--axis of rotation

(4) Computation procedures. First, select an arbitrary amount of flow for the harmonic flow. Then, on the basis of the condition of mutual equality of static pressures between the main flow and the harmonic flow, make a precise determination of the expansion of the main flow in the exhaust of the main jet tube. The precise determination of the points on the boundary lines of the two flows involved is done by the use of the successive substitution method. In this method, as far as the static pressure of the harmonic flow is concerned on the one hand, we write out the continuity equations for two cross sections of the harmonic flow and, on the other hand, we write out the equation for the characteristic curve which appears in the vicinity of these points. These calculations are continued straight on to the exhaust of the jet tube.

If one is dealing with the case in which the harmonic flow is subsonic, then the determining condition is that the static pressure of the harmonic flow in the exhaust of the jet tube is equal to the surrounding atmospheric pressure. When the harmonic flow in the exhaust plane is supersonic, then the harmonic flow has a throat section and the M number for this cross section is 1. The determining condition at this time is the identity of the amount of flow which is selected with the amount of flow which is capable of passing through the throat section of the jet tube.

3. The adjustment for the influence of viscosity [3,4,7]. As far as the subject of the influences of viscosity is concerned, reference [4] is concerned with the adjustment of the area of the cross section of the throat section of the harmonic flow in terms of its shape. Reference [3] then concerns itself with adjustments for the influence of the boundary lines of the main flow and the harmonic flow as well as with such adjustments for the influences of the boundary layers on the external walls. The former method is simple; however, the degree of accuracy is less than excellent. The latter method of adjustment is relatively complicated. What this article presents as the best solution is a method of adjusting the coordinates of the shroud. The procedure for this method is (1), on the basis of the dimensions of the original ejector nozzle shroud, calculate the non-viscous flow field, (2) calculate the displacement thickness of the mixture layer between the main flow and the harmonic flow, (3) calculate the displacement thickness of the boundary layer on the inner walls of the shroud, (4) from the dimensions of the harmonic flow passage cross section which was calculated on the basis of the non-viscous flow field, subtract the displacement thickness of the boundary layers involved, then add the displacement thickness of the mixing layer and get the dimensions of the harmonic flow passage cross section after it has been adjusted. After you have done this, adjust the coordinates for the wall surfaces of the shroud, (5) on the basis of the coordinates of the wall surfaces of the shroud after they have been adjusted, make

another use of the method which was used to make the non-viscous calculations and use it this time to calculate the entire flow field. The details of the calculations are as follows:

(a) Concerning the calculation of the displacement thickness of the mixing layer of the harmonic flow, δ_1^* , if one recognizes the fact that the mixing layer is isobaric, then the speed diagram Fig. 5 for the interior of the mixing layer can be obtained from the various equations below [4], that is

$$\begin{aligned}\varphi - u/u_a &= (1 + \varphi_b)/2 + [(1 - \varphi_b)/2](1/\pi^{1/2}) \left(\int_0^\eta e^{-\beta^2} d\beta \right) \\ &= (1 + \varphi_b)/2 + [(1 - \varphi_b)/2] \operatorname{erf} \eta\end{aligned}\quad (13)$$

In these equations, $\varphi_b = u_b/u_a$, u_b is the speed of harmonic flow, u_a is the speed of the main flow and $u - x$ are the directional components of velocity.

$$\operatorname{erf} \eta = (2/\pi^{1/2}) \int_0^\eta e^{-\beta^2} d\beta,$$

$\eta = \sigma(y/x)$. σ is the equivalence parameter and it is obtained from the empirical radius formula. y and x are the coordinates in the coordinate system within the layer of mixing. The flow speed at the point at which $y = 0$ is $u = (u_a + u_b)/2$, that is, $\varphi = (1 + \varphi_b)/2$.

η is the equivalent coordinate, that is to say that it is only necessary for the value of y/x to be the same and then the value for u/u_a will also be the same. That is the same thing as saying that the speed diagrams for the various cross sections of the mixing layer are all similar.

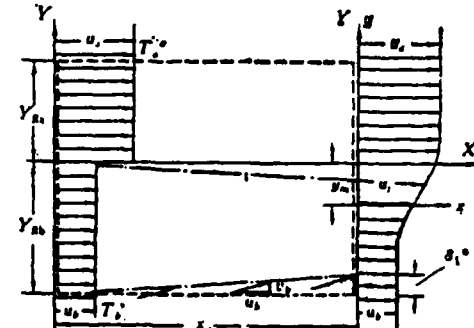


Figure 5. A speed chart for the interior of the mixing layer

If we select the Prandtl number to be 1, and ignore $\partial p/\partial z$, as well as assuming that C_p is a constant, then it is possible, from the speed diagrams, to directly obtain the diagrams of temperature, that is to say,

$$\Lambda = T^*/T_b^* = [1/(1 - \varphi_b)][(T_a^*/T_b^*) - \varphi_b + (1 - T_a^*/T_b^*) \cdot \varphi] \quad (14)$$

In these equations, T^* is the total temperature inside the mixing layer. T_a^* is the total temperature of the main flow. And T_b^* is the total temperature of the harmonic flow.

If we are dealing with a case in which we already know the speed, temperature and static pressure of the various points inside the mixing layer (the static pressure is equal to the static pressures of the main and harmonic flows on the boundaries of the mixing layer), then it is possible to solve for the displacement thickness of the mixing layer. The speed diagrams and temperature charts which were spoken of above are both given in the form of values of x , y coordinates in the internal coordinate system. The relationship between these and the coordinates of the reference coordinate system x , y is $Y = y - y_m$. The jet boundary lines within the mixing layer use i for their representation (see Figure 5). As far as the point at which $y = y_i$ is concerned, it is best to take the mixing layer and divide it up into two sections. It is best that the amount of flow which goes through the range from η_i to η_{Rb} be equal to the amount of main flow which enters the mixing layer. On the basis of the momentum and mass of the mixing layer and analysis of these two quantities in light of the principles regarding their conversation, we can solve for η_i , that is

$$\begin{aligned} I_i(\eta_i) &= [I_i(\eta_{Rb}) - I_i(\eta_{Rb})]/(1 - \varphi_b) \\ I_i(\eta) &= [(1 - C_e^2)\varphi_b\eta_{Rb}]/[(T_a^*/T_b^*) - C_e^2\varphi_b^2] \\ &\quad + \int_{\eta_{Rb}}^{\eta} [(1 - C_e^2)\varphi/(A - C_e^2\varphi^2)]d\eta \\ I_i(\eta) &= [(1 - C_e^2)\varphi_b\eta_{Rb}]/[(T_a^*/T_b^*) - C_e^2\varphi_b^2] \\ &\quad + \int_{\eta_{Rb}}^{\eta} [(1 - C_e^2)\varphi^2/(A - C_e^2\varphi^2)]d\eta \end{aligned} \quad (15)$$

In this equation, C is the Clark number. Concerning the relationship $C^2 = M^2/[2/(\kappa - 1) + M^2]$, Y_m is also solved for on the basis of the principle of the conservation of mass and momentum and is given by the use of similar coordinates, that is

$$\eta_m = \sigma y_m/x = \eta_{Rb} - [1/(1 - \varphi_b)][I_i(\eta_{Rb}) - \varphi_b I_i(\eta_{Rb})] \quad (16)$$

According to the concept of the displacement thickness of boundary layers, one gets the displacement thickness of the harmonic flow of the mixed region, δ_{mixing}^* in the form

$$-\sigma \delta_{\text{mixing}}^*/x = \sigma v_b/u_b = [(T_b^*/T_{\infty}^*) - C_b^* \varphi_b] l_1(\eta_b) / [(1 - C_b^*) \varphi_b] - \eta_m \quad (17)$$

In this equation,

$$\begin{aligned} \sigma &= (\sigma/\sigma_1) \cdot \sigma_1, \text{ where } \sigma_1 = 12 + 2.758 C_{st} / \sqrt{(1 - C_{st}^2)^{k_1-1/2}}; \\ k_1 &= [k_0 + (G_{\infty} \sqrt{T_b^*}) / (G_{\infty} \sqrt{T_{\infty}^*})] / [1 + (G_{\infty} \sqrt{T_b^*}) / (G_{\infty} \sqrt{T_{\infty}^*})]; \\ \sigma/\sigma_1 &= (1 + \varphi_b) / (1 - \varphi_b); C_{st} = C_b^* (1 - \varphi_b) / [C_b^* (1 - \varphi_b)^2 + (1 - C_b^*)]. \end{aligned}$$

(b) The calculation of the displacement thickness, $\delta_{\text{boundary}}^*$ of the boundary layers on the wall surface inside the shroud. If we use the displacement thickness $\delta_{\text{boundary}}^*$, of the boundary layers to estimate the influence of the boundary layers on the inner walls of the shroud on the amount of the harmonic flow, then the properties of the boundary layers are calculated on the basis of an equivalent length and this equivalent length is defined as

$$x = (Gy^*)^{-1} \int_0^x (Gy^*) dx \quad (18)$$

In this equation $G = [M/(1 + 0.2M^2)]^{\beta}$, and β is selected as 1.20 or 1.25, depending on the Reynolds number. The Reynolds number which corresponds to the equivalent length as determined by the equation above, that is, R_x is calculated by using the total pressure and total temperature, that is to say

$$R_x = [\sqrt{k_B RT^*} / r^*] M, (1 + 0.2M^2)^{-1.25} \quad (19)$$

In this equation $r^* = 9.81 T^* R [\mu(T^*) / p^*]$. Concerning the use of the corresponding Reynolds number, R_x , to calculate the displacement thickness $\delta_{\text{boundary}}^*$ and the momentum thickness θ , when the order of R_x is 10^6 , then we use the equations below to express the relationships involved, that is

$$\delta_{\text{boundary}}^* = 0.046 x (1 + 0.8M^2)^{0.44} R_x^{-0.25} \quad (20)$$

$$\theta = 0.036 x (1 + 0.1M^2)^{-0.70} R_x^{-0.25} \quad (21)$$

When the order of R_x is 10^7 , then use the equations below in order to express the relationships involved, that is

$$\delta_s^* = 0.028x(1.0 + 0.8M_f^2)^{0.4} R_s^{-0.167} \quad (22)$$

$$\theta = 0.022x(1.0 + 0.1M_f^2)^{-0.70} R_s^{-0.167} \quad (23)$$

These equations above are accurate for $k = 1.4$. Due to the fact that we recognize that the static pressure inside of the boundary layers involved is a constant, when we calculate the pressure of the separation surface δ^* , it is possible to recognize the fact that what we are figuring is the surface pressure and this pressure acts as the basis for a repeated substitution. Because of this, as far as these calculations are concerned, it is possible to carry them out, in their cyclical form, using a standard coordinate form which is the same as the one on the surface.

4. The calculation of thrust performance [5]. Engine thrust is given by the relationships set out below, that is

$$R = (G/g)V_e + p_e A_e - p_H A_e - (G/g)V_0 = R_G - (G/g)V_0 \quad (24)$$

In this equation R_G is the total thrust, that is

$$R_G = F_e - p_H A_e$$

On the basis of the theorems relating to momentum, the equation above can be changed to be

$$R_G = F_e + F_b + R_{sh} - p_H A_e \quad (25)$$

and

$$F_e = x(\lambda_w)(1.0 + k_f c_D c_v M_\infty^2) A_e p_e^* \quad (\text{此处 } M_\infty = 1) \quad (26)$$

$$F_b = p_b \cdot A_b (1.0 + k_b M_\infty^2) c_a \quad (27)$$

$$R_{sh} = \int_0^{x_L} (p_b \cdot 2\pi y \lg(\phi_{sh}) + c_a \cdot \pi \cdot y k_b p_b M_f^2 \sqrt{1 + \lg^2(\phi_{sh})}) dx \quad (28)$$

In these equations, c_f is the coefficient of friction of the wall surfaces of the shroud. c_D is the coefficient of flow of the main jet tube. c_v is the speed coefficient of the main jet tube. And, y is the wall surface radius of the shroud.

When one is considering the influence of viscosity, the coefficients for the speed and the amount of flow are solved for

respectively by the use of the equations presented below, that is

$$c_D = \left[\int 2\pi y (\cos \phi dy - \sin \phi dx) \right] / \int 2\pi y dy \quad (29)$$

$$c_s = \left[\int 2\pi y (\cos \phi dy - \sin \phi dx) \cos \phi \right] / \left[\int 2\pi y (\cos \phi dy - \sin \phi dx) \right] \quad (30)$$

The integrations in these equations are carried out along the sonic line. If one is considering the influence of viscosity, then the coefficients of speed and amount of flow for the main jet tube have formulae which are respectively

$$c_D = (1.0 - k_1 R_c^{-0.2}) \left[\int 2\pi y (\cos \phi dy - \sin \phi dx) \right] / \int 2\pi y dy \quad (31)$$

$$c_s = (1.0 - k_2 R_c^{-0.2}) \left[\int 2\pi y (\cos \phi dy - \sin \phi dx) \cos \phi \right] / \left[\int 2\pi y (\cos \phi dy - \sin \phi dx) \right] \quad (32)$$

In these equations, $k_1 = 0.185/\cos \alpha$; $k_2 = 0.144$; ϕ is the included angle between the flow speed on the sonic line and the x axis. y is the vertical coordinate for points on the sonic line. x is the horizontal coordinate for points on the sonic line. And R_c is the Reynolds number

A COMPARISON BETWEEN THEORETICAL CALCULATIONS AND EXPERIMENTAL RESULTS

Concerning the use of the computational methods and sequence which are presented in this article, we used them to calculate the ejector nozzle flow field, the wall surface pressure distribution and the pumping performance of the jet tube. Moreover, we made a comparison of these calculated results with the results from experiments involving model simulations of the jet tubes involved. The results of this comparison are as shown below.

1. The flow field and wall surface pressure distribution of a jet ejector nozzle.

The curve network for the performance of an ejector nozzle, as it was calculated, is as shown in Figure 6. The calculated values for the pressure distribution on the wall surfaces of the shroud and the results of the related experiments are as shown in Figure 7.

2. The pumping performance of the ejector nozzle.

As Figure 8 shows, curve 1 represents the results of calculations of the non-viscid flow and curve 2 is the result after this original curve is corrected for the effects of viscosity. Figure 8 shows that, after the adjustments for viscosity are made, the theoretical and experimental results are basically the same. Figure 8 also shows that when one is working with a situation in which there is a high harmonic flow, the error which appears between the non-viscous flow calculations and the data obtained through experimentation does not exceed 10%.

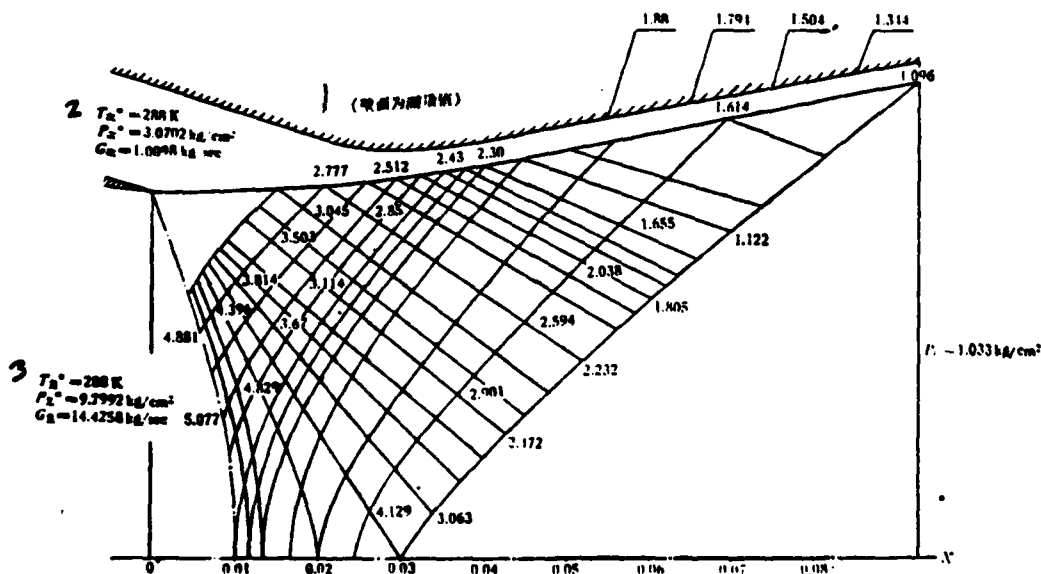


Figure 6. A graph of the performance curve network for the ejector nozzle under consideration.

1--the wall surface is the measured value; 2--harmonic; 3--main

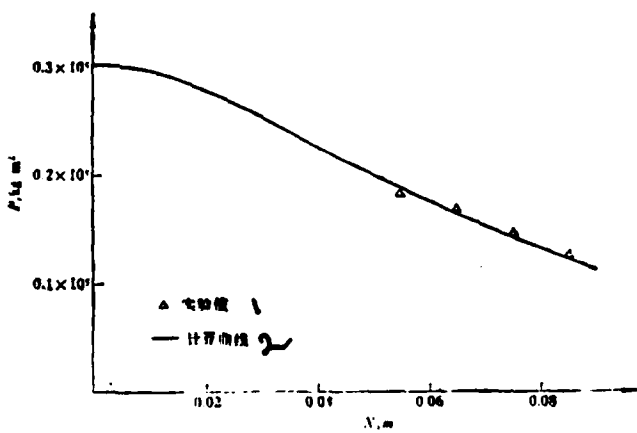


Figure 7. The pressure distribution of the wall surface of the shroud.
 1--experimental values; 2--calculated curve

CONCLUSIONS

1. There is an adequate correlation between the calculation methods introduced in this article and the experimental results obtained for the same values.
2. The method which the article presents for viscosity corrections is relatively simple and is, at the same time, adequately accurate.

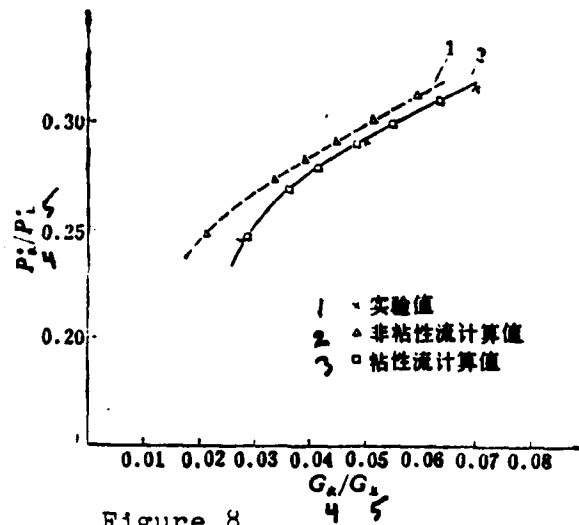


Figure 8

1--experimental values; 2--calculated values for non-viscous flow;
 3--calculated values for viscous flow

TABLE OF SYMBOLS

ψ	flow function	ξ	coordinates on the Mach line
ρ	density	β	constant whose selection is dependent on the Reynolds number
a	speed of sound	γ^*	a viscosity coefficient represented by the use of a blockage coefficient
u	axial speed	s_+^*	the displacement thickness of boundary layers (+ = boundary)
v	radial speed or the flow speed in the exhaust of the engine		
p	pressure		
μ	Mach angle		
ϕ	flow line angle (the included angle between the flow line involved and the horizontal axis)		
θ	the included angle between the characteristic curve and the vertical axis or the boundary layer momentum thickness		
X	equivalent length		
y	radial distance divided by the radius of the jet nozzle		
x	axial distance divided by the radius of the jet nozzle		
ω	transform speed		
α	hemipyramidal angle of the exhaust of the jet nozzle		
T	temperature		
G	amount of flow		
M	Mach number		
λ	coefficient of flow speed		
k	specific heat ratio		
R	thrust or gas constant or radius		
A	area		
F	impuse or functional relation		
n	coordinates on the Mach line		
			Subscripts
		a	pertaining to the main flow
		b	pertaining to a harmonic flow
		c	main jet tube exhaust
		e	cross section of engine exhaust
		H	boundary conditions
		G	total
		O	engine intake
		s^H	shroud
			Superscripts
		*	blockage coefficient

REFERENCES

- [1] Hardy, J. M.: Étude Théorique d'une Turère Convergente-Divergente Bi-Flux, L'Aéronautique et L'Astronautique, No. 37, 1972-5, pp. 28—37.
- [2] Hardy, J. M., et Lacombe, H., Les Tuyères Supersoniques à Double Flux. Méthodes de Calcul, Revue Française de Mécanique, No. 24, 4 trimetre, 1967, pp. 49—59.
- [3] Anderson, B. H.: Computer Program for Calculating the Field of Supersonic Ejector nozzles, NASA TND-7601, 1974, pp. 1—88.
- [4] Chow, W. L. and Addy, A. L.: Interaction between Primary and Secondary Streams of Supersonic Ejector Systems and Their Performance Characteristics, AIAA Journal, Vol. 2, No. 4, April 1964, pp. 686—695.
- [5] Korst, H. H., Addy, A. V. and Chow, W. L.: Installed Performance of Air-Augmented Nozzles Based on Analytical Determination of Internal Ejector Characteristics, Journal of Aircraft, Vol. 3, No. 6, Nov.-Dec. 1966, pp. 498—506.
- [6] Carriere, P.: Exhaust Nozzles. Supersonic Turbo-jet Propulsion Systems and Components, AGARD graph No. 120, 1969, pp. 287—374.
- [7] Anderson, B. H.: Factors which Influence the Analysis and Design of Ejector Nozzles, AIAA, Paper 72—46, Jan. 1972.

ANALYTICAL AND EXPERIMENTAL INVESTIGATION OF PERFORMANCE OF SUPERSONIC EJECTOR NOZZLE

Shen Hui-li, Chen Zhong-qing
(North-Western Polytechnical University)

Abstract

This paper presents an analytical method for calculating the flow field and performance of supersonic ejector nozzle. The calculations involve the real sonic line at the exit of the primary nozzle, the inviscid primary flow field, the correction for viscosity effect and the pumping, and thrust characteristics.

In order to bring calculated results into agreement with experimental data, the real sonic line, instead of the plane sonic line, is taken as the initial base line of calculation. The real sonic line is obtained by joining the points of intersection of constant flow angle lines in the throat region with Mach lines at the lip of the primary nozzle.

First, the inviscid primary flow field of the nozzle is calculated and then corrected to account for the viscosity effect. The method of correction for viscosity effect proposed in this paper replaces the original geometric coordinates of the ejector shroud with corrected geometric coordinates, which are obtained by superimposing on the original geometric coordinates the displacements of the mixed region and the boundary layer. On the basis of the corrected coordinates, the actual primary flow field and pumping performance of the nozzle are then calculated. The proposed method proves to be quite simple and accurate.

Calculations were performed on a "320" digital computer, and model tests on a ground test facility. The analytical and experimental results are found to be in fairly satisfactory agreement.

ANALYTICAL AND EXPERIMENTAL INVESTIGATION
OF SUPERSONIC EJECTOR NOZZLE*

Wu Da, Yang Zai-ming and Zhang Rung
(Beijing Institute of Aeronautics & Astronautics)

SUMMARY

In this article, we introduce some test results concerning ejector nozzles and, on the basis of these results, we offer a simplified model of flow configuration within ejector nozzles. On the basis of this model, we based approximation formulae with which to calculate the thrust performance within these nozzles. Finally, we carried out actual test calculations and took the results of these calculations and compared them to actual measured values. The results of this process showed that the calculated values and the measured values were in sufficient agreement with each other.

1. PREFACE

Concerning supersonic ejector nozzles, because of the fact that their structure is simple and compact, in situations where one is dealing with large drops in pressure, these nozzles have excellent characteristics. Because of this, they are widely used in supersonic fighters, bombers, transport planes and civilian aircraft.

Because of the fact that the requirements of various types of aircraft are not the same, the differences in structure between different types of ejector nozzles are very great. If we speak in terms of the actual types of hardware involved, a small number of possible structural designs is chosen, after careful comparison and selection from among a large number of original types of design possibilities, after these possible designs have gone through static state testing of the ejector nozzles involved. This is the normal procedure. If one operates in this way, one finds that, in such

*This paper was read at the 2nd Annual All-China Engineering Thermophysics Technology Conference in Hangzhou in November of 1978.

related areas as design plans, the machining of test components and the organization of experiments, the amount of work expended is large, the development periods involved are long and the procedure is not economical. It cannot be doubted that, if one were able, in the initial selection of a design, to make performance estimates of various different types of design plans, in order to weed out those designs whose performance was relatively unsatisfactory, and because of this preselection process, only have to organize evaluation tests for a small number of designs, that the process of selecting the best design could be made faster, better and more economical.

In the last few years we have, on a floating sleeve type test bed for the evaluation of perpendicular intake ejector nozzles, made tests on several score of different structural models for ejector nozzles, photographed several types of these, as well as the flow spectra for these nozzles under different types of flow conditions. Moreover, we carried out analyses of these experimental data and flow spectra and came up with types of models for the interior of ejector nozzles under different conditions of flow configuration. On the basis of these models, we set up methods for the estimation of the interior performance of the ejector nozzles being evaluated. What follows is a discussion of the main experimental results which we got and the performance analyses we did.

2. A THEORETICAL ANALYSIS OF THE INTERIOR CHARACTERISTICS OF SUPERSONIC EJECTOR NOZZLES

(one) Thrust characteristics for the interiors of ejector nozzles.

On the basis of an analysis of the flow spectra of the ejector nozzle exhaust flow of ejectors being tested, we offer a type of flow model for main jet nozzles placed in configurations of incomplete (or complete) expansion, and we make the following assumptions.

With this done, it is possible to carry out calculations of the thrust characteristics inside of ejector nozzles.

1. Concerning the common boundary between the main flow and the harmonic flow(s), that is, the body of revolution which is formed by the elliptical curve is the form of the column of the main flow.

2. During the time in which the flow inside the ejector nozzle is expanding and accelerating, we accept the fact that the nozzle is in a flow configuration of complete stability, that is to say that the working fluid does not give rise to a separation into components and the specific heat remains constant.

3. There is no heat exchange between the main flow and harmonic flows.

4. During flow, the most important consideration is shock wave losses.

5. We recognize the fact that the gas flow in the ejector nozzle functions as an adiabatic energy-insulated flow.

6. The harmonic flow(s) act as one-dimensional, isoentropic flows.

Figure 1 is the shadow photograph of the flow spectrum of the exhaust of the ejector nozzle which we were considering in three different cases (these three cases can be seen in schematic diagram Figure 2). From this set of photographs, it can be seen that, under differing types of pressure loss ratios, the main flow always maintains within itself the existence of a shock wave and following a reduction in the ratio of pressure drop, the shock wave continuously moves in toward the nozzle sleeve of the ejector nozzle. In this condition, the shock wave also gains in strength. In order to make the analysis more convenient, we took the flow configurations inside

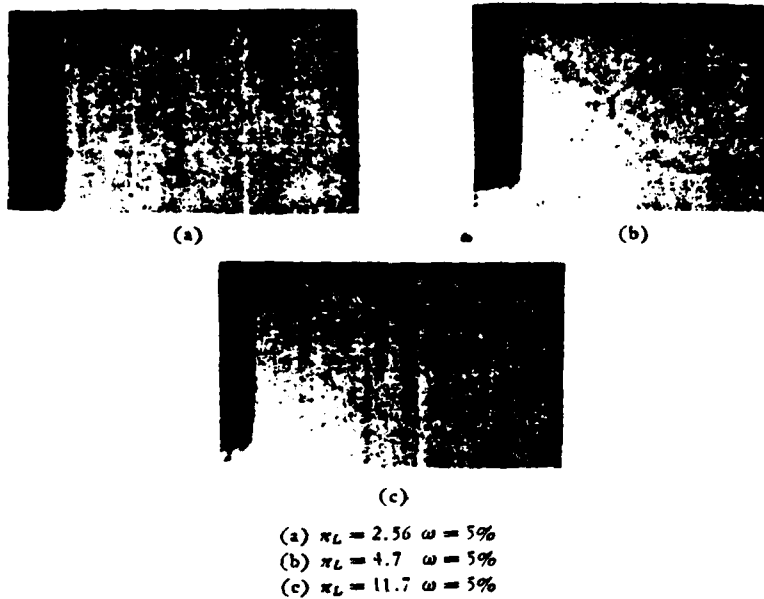


Figure 1. The flow configuration when different pressure drop ratios are in effect for expansion type outer tube sleeves

ejector nozzles for different pressure drop ratios and simplified them by using the models which are shown in Figure 2.

When the pressure drop ratio for the main flow is larger than the design value, that is, when ($\pi_t > \pi_{t,i}$) , then, the ejector nozzle is put into an incomplete expansion operational configuration, and the main flow acts as an isoentropic flow inside the tube sleeve. The shock wave in the main flow makes its appearance in the free jet in the ejector nozzle. Concerning the position of the largest horizontal tangential surface in the column of the main flow, this may easily appear at a certain place outside the exhaust of the ejector nozzle and the actual position of it is related to the pressure drop ratio.

In order to improve the performance of ejector nozzles under conditions in which the pressure drop ratios are low, it is only necessary to have, when one approaches the design pressure drop ratio, the main flow in the ejector nozzle, and it will approach

complete expansion. In this type of flow configuration, the largest horizontal tangential surface in the main flow column is located on a tangential surface close to the exhaust of the tube sleeve.

It makes no difference if the main flow is placed into an incomplete expansion configuration or into a complete expansion configuration, the tangential surface to the exhaust of the ejector nozzle is filled up with lower harmonic flow and with supersonic main flow which has not passed through the shock wave.

When the main flow is in the condition $\pi_L < \pi_{c,i}$, and the main jet nozzle is still in operation with the pressure drop at levels beyond the critical stage, that is $(\pi_c > \pi_{c,i})$, then in such a situation, the ejector nozzle is placed into an over-expansion configuration. In this type of condition, the main flow leaves the main jet nozzle and immediately wraps itself around the edges of the exhaust, that is, it immediately goes into Prandtl-Meyer expansion. From the critical pressure value of the exhaust of the main jet nozzle, it immediately expands to the point where the edges of the main jet nozzle are placed in a static pressure of harmonic flow. After the main flow crosses the Class II expansion characteristic curve, and then, also crosses the Class I expansion characteristic curve which appears from the opposite side, it is then, and only then, that it stops progressively expanding. Because of the fact that the form of the common boundary between the main flow and the harmonic flow(s) is most certainly not congruent with the surface form which is required by the ideal expansion of the main flow. In this way, when the expansion characteristic curve reaches the common boundary surface, it will reflect from the common boundary surface weak shock waves. These weak shock waves gather together and they form, at a place which is not far from the common boundary surface, a relatively strong shock wave. When the gas flow passes across the shock wave we just mentioned, there is created a turning in the opposite direction. Moreover, on the largest tangential surface to the column of

the main flow, the gas flow also turns back to the same direction that the axis has. It can be seen from this that, in configurations in which we have excessive expansion, the position of the largest horizontal tangential surface to the column of the main flow is placed inside the tube sleeve of the ejector nozzle. Moreover, on the tangential surface to the exhaust of the ejector nozzle, we take the main flow and divide it into two parts, that is to say, the center flow which has not passed through the shock wave and the exterior flow which has passed through the shock wave.

On the basis of what has been said above, it is possible to set up the necessary equations. We recognize the fact that the common boundary surface between the main flow and the harmonic flow(s), that is to say, the main flow jet column is related to the body of revolution which is formed by the elliptical curve and its gear profile as well as to the pressure drop ratio π_L and the flow ratio ω .

Because of these facts, the cylinder of the main flow jet can be described by the use of this equation

$$\frac{x^2}{(R_{zzd}^2 - R_z^2)R_{zzd}^2/\gamma g^2 \theta R_z^2} + \frac{y^2}{R_{zzd}^2} = 1 \quad (1)$$

In this equation, R_{zzd} is the radius of the largest horizontal tangential surface to the column of the main flow and, on the basis of experimental data, it is possible to adjust it to be

$$R_{zzd} = R_s \sqrt{1 + K(\pi_L - \pi_{LJ})} \quad (2)$$

Experimental results demonstrate that, within the range $\pi_L < 8 - 10$, $\omega = 0.02 - 0.04$ it is possible to select $K = 0.18$.

The angle θ in Equation (1) is the angle of slope of the cylinder of the main jet at the exhaust of the main jet nozzle. This is determined by the expansion of the pressure which is found on the tangential surface of the main flow at the exhaust of the main jet nozzle expanding into the pressure which is found in the surrounding

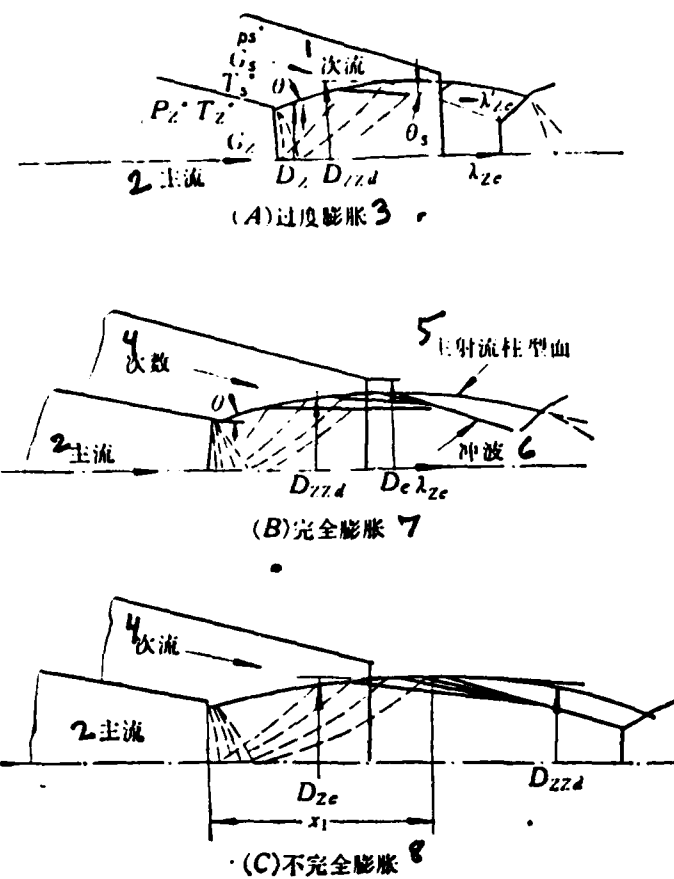


Figure 2. Simplified models of ejector nozzles under different flow configurations.
 1--harmonic flow; 2--main flow; 3--excessive extension; 4--harmonic flow; 5--cylindrical surface of the main jet; 6--shock wave; 7--complete expansion; 8--incomplete expansion

harmonic flows, that is to say, $\theta = f(p_e/p_e^*)$ (when $p_e = p_e^*$, it is it is possible to select $\theta = f(p_e^*/p_e^*)$). Due to the fact that the main flow, at the exhaust of the main jet nozzle, suddenly expands around the outside obtuse angles, the main flow, which expands in three dimensions, can be usefully illustrated in two dimensions.

From this it is possible to fix the distance x_1 which separates the largest horizontal tangential surface of the main jet cylinder from the edge of the exhaust of the main jet nozzle.

$$x_1 = (R_{zzd}^2 - R_e^2) / 4\theta R_e \quad (3)$$

In an incomplete expansion type situation, $x_1 > L$, that is to say that the largest tangential cross section of the cylinder of the main flow is located outside of the exhaust of the ejector nozzle. The radius of the main flow cylinder on the tangential plane of the exhaust of the ejector nozzle is

$$R_{\infty} = R_{ext} \sqrt{1 - \frac{(x_1 - L)^2 g^2 \theta R_i^2}{(R_{ext}^2 - R_i^2) R_{ext}^2}} \quad (4)$$

Once again, on the basis of the continuity conditions of the main flow contained in the relationship $\pi(\lambda)$, it is possible to obtain all the physical parameters as well as the tangent planes of the path of flow on the tangent plane of the exhaust of the ejector nozzle for the main flow.

In this sort of operational configuration, the tangent plane which is occupied by the harmonic flow on the tangent plane to the exhaust of the ejector nozzle is

$$A_n = \pi(R_i^2 - R_{\infty}^2) \quad (5)$$

Concerning the flow speed of the harmonic flow at the exhaust of the ejector nozzle, this can be obtained from the equation for the amount of flow

$$q(\lambda_n) = \omega \frac{\rho_i^2 A_n m_i C_s}{\rho_i^2 A_{ext} m_i C_s} \quad (6)$$

In a tube sleeve with a contracted form, the greatest speed of flow of the harmonic flow at the exhaust is $\lambda_{ext} = 1$. Generally speaking, when the pressure drop ratio and the ratio of the amounts of flow are not too large, that is

$$(\omega = (G_s/G_i) \sqrt{T_i^* / T_s^*})$$

then, the flow speed of the harmonic flow in the tangent plane to the exhaust of the tube sleeve is always subsonic.

In this type of case, that is, when the main flow is in a condition of complete or incomplete expansion, and the flow speed of the harmonic flow at the exhaust has not reached a critical value, the actual thrust which is produced at the ejector nozzle is $F = F_z + F_s$, that is to say

$$F = p_i^* A_{se} f(\lambda_{se}) \eta_{se} + A_{se} [p_e(1 - \eta_{se}) - p_u] + A_{se} \eta_{se} [p_i^* f(\lambda_{se}) - p_u] \quad (7)$$

In this equation, η is the corrected thrust parameter as derived from the ideal theoretical parameter which does not take into consideration the effects of boundary layers. For the respective cases of the main and harmonic flow, this parameter is

$$\begin{aligned} \eta_{se} &= C_s \cdot C_d \\ \eta_{se} &= C_s \cdot C_d \end{aligned} \quad (8)$$

C_d , C are respectively the parameters for the amount of flow and momentum losses as determined by experimentation. When the main flow is in an excessive expansion configuration, as a function of a drop in the pressure drop ratio, the shock wave(s) moves up the path of the gas flow as far as the upper reaches of the flow. Because of this, in a situation in which there is a relatively low pressure drop ratio, the shock wave is capable of entering as far as the inside of the tube sleeve of the ejector nozzle. At such a time, the largest horizontal tangent plane to the cylinder of the main flow is located within the tube sleeve. The shock wave takes the main flow and divides it up into two parts on the tangent plane to the exhaust of the tube sleeve, that is to say, into the center flow in front of the shock wave and the external flow behind it.

The flow speed of the central flow in front of the shock wave is obtained from the continuity condition

$$q(\lambda_{se}) = (R_s/R_{se})^2 \quad (9)$$

Its static pressure is

$$p_{se} = p_i^* \pi(\lambda_{se}) \quad (10)$$

λ'_{zc} for the main flow behind the shock wave is determined by the strength of the shock wave. The reason for this is that, when one is dealing with the type of situation, one can recognize the fact that after this section of the flow goes through the cone of the shock wave, its static pressure goes up to that of the atmospheric pressure P_H on the external boundary. The shock wave angle θ_s can be determined from the pressure rise ratio P_H/P_{zc} and the speed in front of the wave λ_{zc} . Because of this, it is possible to make use of the related equations which are already known or the graphs of these in order to figure out θ_s , λ'_{zc} as well as the parameter of total pressure losses σ .

In this type of operational configuration, the radius of the main flow cylinder on the tangent plane at the exhaust of the ejector nozzle is

$$R_{et} = R_{ext} \sqrt{1 - \frac{(L - x_1)^2 \tan^2 \theta R_s^2}{(R_{ext}^2 - R_s^2) R_{ext}^2}}$$

By making use of geometrical relationships, we can figure that the area of the tangent plane which is occupied by that part of the main flow which has not gone through the shock wave is

$$\begin{aligned} R_{et} &= R_{ext} - (L - x_1) \tan \theta, \\ A_{et} &= \pi R_{et}^2 \end{aligned} \quad (11)$$

The area of the tangent plane at the exhaust of the tube sleeve which is occupied by that part of the main flow which has passed through to the other side of the shock wave is

$$A_{ext} = \pi (R_{et}^2 - R_{ext}^2) \quad (12)$$

Because of these facts, when one is operating in a situation of excessive expansion, the actual thrust which is produced by the ejector nozzle is

$$F = F_{et} + F_{ext} + F_e$$

that is to say,

$$F = p_m^* A_{sel} f(\lambda_{sel}) + p_h^* \sigma A_{sel} f(\lambda'_{sel}) \eta_{se} + \frac{p_h A_{se}}{r(\lambda_{se})} \eta_{se} - p_h (A_{se} + A_{sel} \eta_{se} + A_{se} \eta_{se}) \quad (13)$$

In this way, when one considers ejector nozzles with already given geometrical forms to their external shapes as well as $p_m^*, p_h^*, T_m^*, T_h^*, \omega$ of the main and harmonic flows and the properties of the main and harmonic flows k, m , then it is possible to calculate the actual thrust which is produced when the ejector nozzle under consideration is operating under different configurations. And from this, we can go on to figure out the relationship between this thrust and the pressure drop ratio, that is to say, the thrust performance inside the ejector nozzle under consideration.

(Two) The actual thrust inside of the ejector nozzle

If one looks at Figure 3, it can be seen that the solid wall surfaces which the main and harmonic flow wrap themselves around are all show the presence of the formation of boundary layers. Concerning the area of mixing, from the trailing edges of the main jet tube onward, when the main flow and the harmonic flow begin to come in contact with each other, they flow on smoothly in the direction of the air flow, expanding as they go until they reach the exhaust of the ejector nozzle. The thickness of the area of mixing is δ_c and its thickness of momentum loss is δ_c^{**} . If we make use of the laws governing momentum, we accept the condition of ignoring the shear forces on the boundaries of the area of mixing. Concerning the flow within the area of mixing, it is possible to use this type of impulse equation in order to describe the situation

$$\frac{d\delta^{**}}{\delta^{**} dx} + \frac{dp_s}{\rho_s dx} + (2 + \delta^*/\delta^{**}) \cdot \frac{dV_s}{V_s dx} = 0 \quad (14)$$

If we take the parameter for the form of the surface $H = \delta^*/\delta^{**}$ for purposes of expression and we take the fixed values of $H_{pj} = (H_z + H_{zc})/2$ for purposes of substitution, then the equation above can be directly integrated and, after it has undergone simplification

we can obtain the thickness of momentum loss, δ_c^{**} , on the tangent plane at the exhaust of the ejector nozzle is

$$\begin{aligned}\delta_c^{**}/\delta_{in}^{**} &= \rho_s/\rho_{in}^* \cdot \frac{1}{(\rho_{in}/\rho_{in}^*) \cdot \lambda_{in}^{(2+H_{pi})}} \\ &= [2/(k_s + 1)]^{1/k_s - 1} \cdot \frac{1}{\left(1 - \frac{k_s - 1}{k_s + 1} \lambda_{in}^2\right)^{1/k_s - 1} \cdot \lambda_{in}^{(2+H_{pi})}}\end{aligned}\quad (15)$$

From the equation above, it can be seen that, as far as the thickness of momentum loss at the exhaust of the ejector nozzle goes, besides the fact that it is related to the way in which the main flow expands, this thickness is also determined by the parameter for the average surface form H_{pc} . In order to make a precise determination of the thickness of momentum loss at the exhaust of the jet nozzle for the region of mixing, that is δ_c^{**} , we assume that the distributions of speed and temperature in the area of mixing are

$$\begin{aligned}U &= \frac{1}{2} V_s \left(1 + \frac{V_r}{V_s}\right) \left(1 + \frac{1 - V_r/V_s}{1 + V_r/V_s} \cos \pi \frac{Y}{\delta}\right) \\ r &= \frac{1}{2} T_s \left(1 + \frac{T_r}{T_s}\right) \left(1 + \frac{1 - T_r/T_s}{1 + T_r/T_s} \cos \pi \frac{Y}{\delta}\right)\end{aligned}$$

If one makes use of the relationships involving U , T in the equations above as well as of $p/p_z = T_z/T$, then it is possible to obtain

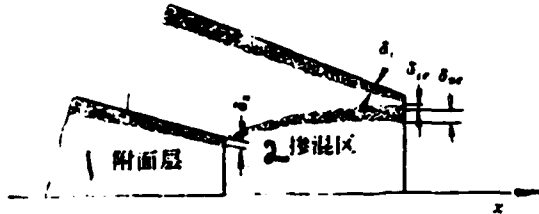


Figure 3. The actual thrust in the ejector nozzle
1--boundary layer; 2--area of mixing

$$H - \frac{\delta^*}{\delta^{**}} = \frac{\int_0^1 \left[1 - \frac{(1 + V_e/V_s) \left(1 + \frac{1 - V_e/V_s}{1 + V_e/V_s} \cos \pi \frac{Y}{\delta} \right)}{(1 + T_e/T_s) \left(1 + \frac{1 - T_e/T_s}{1 + T_e/T_s} \cos \pi \frac{Y}{\delta} \right)} \right] d\left(\frac{Y}{\delta}\right)}{\int_0^1 \frac{(1 + V_e/V_s) \left(1 + \frac{1 - V_e/V_s}{1 + V_e/V_s} \cos \pi \frac{Y}{\delta} \right)}{(1 + T_e/T_s) \left(1 + \frac{1 - T_e/T_s}{1 + T_e/T_s} \cos \pi \frac{Y}{\delta} \right)} \left[1 - \frac{1}{2} \left(1 + \frac{V_e}{V_s} \right) \times \left(1 + \frac{1 - V_e/V_s}{1 + V_e/V_s} \cos \pi \frac{Y}{\delta} \right) \right] d\left(\frac{Y}{\delta}\right)}$$

After adjustments are made, we get

$$H - \frac{\delta^*}{\delta^{**}} = \frac{1 - \frac{A}{B} \frac{1}{\sqrt{1 - D^2}}}{\frac{A}{B} - \frac{1}{2} \frac{A}{B} \frac{A}{\sqrt{1 - D^2}}}$$

In these equations

$$\begin{aligned} A &= 1 + V_e/V_s = 1 + \lambda_e/\lambda_s \cdot \sqrt{T_e^*/T_s^*} \\ B &= 1 + T_e/T_s = 1 + T_e^* \cdot r(\lambda_e)/T_e^* r(\lambda_s) \\ D &= \frac{1 - T_e/T_s}{1 + T_e/T_s} = \frac{1 - T_e^* r(\lambda_e)/T_e^* r(\lambda_s)}{1 + T_e^* r(\lambda_e)/T_e^* r(\lambda_s)} \end{aligned}$$

Because of this, it is possible to get a precise value for the thickness of momentum loss δ_c^{**} at the exhaust of the jet nozzle for the area of mixing, and from this, one can go on to get a precise value for the parameter of adjusted thrust n for a situation in which one is taking mixing into consideration.

3. A COMPREHENSIVE STATEMENT CONCERNING EXPERIMENTATION

(One) A short introduction to experimental equipment

One can see a picture of the test bed in photograph 4 and a schematic diagram of it in Figure 5. It is composed of such components as curved air-guide tubes and main flow passages. Concerning

the main jet tubes and external tube sleeves which were used in the experiments, both types of components were screwed into connections on the test bed. The main flow passages and the curved air-guide tubes used floating tube type connectors. The interval between components was 0.6 mm, and this interval was maintained in order to make it easier for the components involved to float free under the effects of applied thrust. The harmonic flow passages and the main flow flow paths were connected together, and this was done in order to facilitate the process of making the pressure in the harmonic flow passages the same as that in the main flow.

Concerning the dry fresh air which is supplied by the air movement ducts, the largest part of it is put out through the main jet nozzle. A small part of it enters the outside tube sleeve and forms the harmonic flow used in the experiments. The amount of the harmonic flow is changed by the exchange limiter nozzle.

The test bed was equipped with weighted lever mechanisms and these were used to make standard measurements of the system of forces involved in both static and dynamic states.

(Two) Measurement parameters and instruments

We made use of total pressure sensors in order to measure the total pressures of the main flow and the dynamic flow being considered. Besides this, there were drilled, in the wall of the harmonic flow ring cavity and in the wall surface of the air-guide tubes below the limiter nozzle, static pressure holes 1 mm in diameter, and these holes were used for making precise measurements of the static pressure of the harmonic flow.

All the measurements of pressure went through a pressure sensor (type SYD), circulating measurement devices (XJ-100) and the digital recorder (LS-5). It was then directly displayed as numerical pressure values or printed out as pressure data.

Use was also made of force measuring sensors (BLR-1), carrier wave amplifiers (LR-1) and integral type numerical voltage tables (DS-13) as well as of printers (SY-3) in order to make measurements of the thrust affecting the test components.

(Three) Test components and experimental sequence

We made tests of several score of main jet tubes with different exhaust diameters (60-90 mm) and different angles of narrowing (α from 10° - 14°)

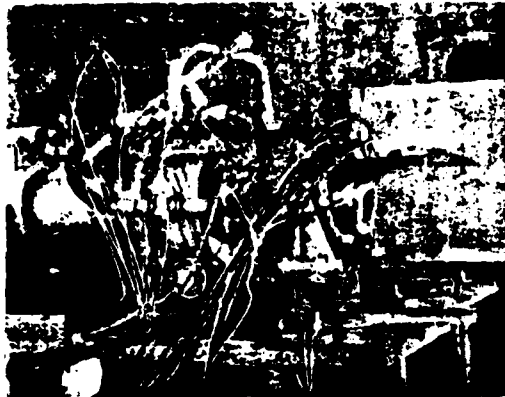


Figure 4. The test bed

We also made tests of several score of different forms of external tube sleeves. These were various sleeves with different forms of narrowing, narrowing and then expanding, sleeves with different diameter ratios (D_e/D_z), different spacing ratios (L/D_z), different angles of sleeve contraction α and sleeve expansion β as well as other similar variable parameters. All these various forms were tested.

All the testing was done within a range in which the ratio of the amounts of flow w is between 1%-7% and the pressure drop ratio is between 1.5 and 14. Moreover, for each value of the ratio of the amounts of flow, continuous experimentation was carried out on the effects of changes in the pressure drop ratio.

4. A COMPARISON OF THE CALCULATED VALUE OF THRUST AND THE EXPERIMENTALLY MEASURED VALUE

We selected the experimental data for tube sleeves with seven different types of narrowing forms and with a spacing ratio L/D_z from 0.58-0.6, and we made a comparison between these results and those thrust values which were obtained by calculation using the methods put forward in this article. The results of this comparison are shown in Figure 6. It can be seen from this illustration that within a very large range of values for the pressure drop ratio of the main flow, these two sets of values agree with each other very well. Figure 7 shows the error between the calculated values and the experimentally determined values as well as the relationship to the pressure drop ratio. It can be seen from this illustration that in practical applications the greatest encountered anywhere is not larger than 4% and the distribution of this error is relatively concentrated. It is only in the case in which the ejector nozzle is placed in an excessive operational configuration that, due to the fact that the form of the flow inside of the tube sleeve is very complicated, there is caused a significant reduction in the accuracy of estimates. Because of the fact that this article considers the characteristics of the actual flows inside of the ejector nozzles under different operational configurations, it raises the accuracy of the estimates of thrust over the entire range of pressure drop ratios. Because of this fact, this method is capable of functioning as something to which engineers can refer when selecting the initial design plans for the structure of ejector nozzles.

5. CONCLUSIONS

The method of analysis of the characteristics of the inside of ejector nozzles which is put forward by this article as well as the corresponding methods for estimating the values of these characteristics have been verified by going through preliminary testing. These methods are, within a very wide range of pressure drop ratios

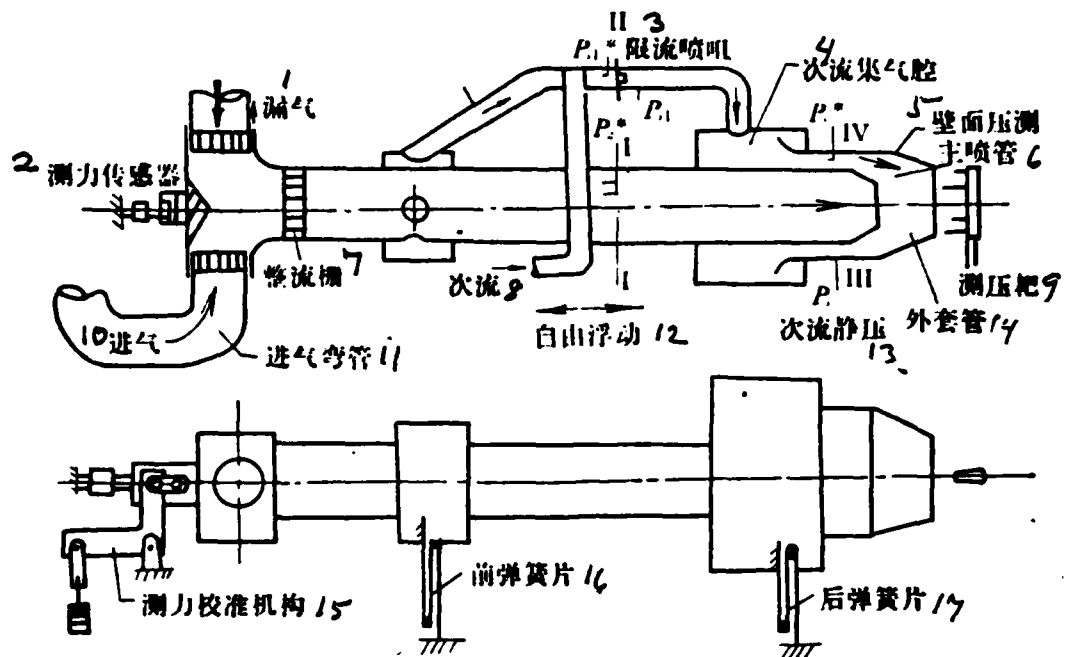


Figure 5. A simplified diagram of the test bed

1--gas leakage; 2--force measuring sensor; 3--flow limiter jet nozzle; 4--harmonic flow collection chamber; 5--wall surface pressure measurement; 6--main jet nozzle; 7--flow rectifier grid; 8--harmonic flow; 9--pressure measuring rake; 10--intake; 11--curved intake tube; 12--free flow; 13--harmonic flow static pressure; 14--external tube sleeve; 15--strength measurement calibration structure; 16--forward sprung plate; 17--backward sprung plate

π_L (approximately from 2.5-14) and ratios of amounts of flow (approximately 1.5%-5%), capable of estimating calculated values of thrust which are in satisfactory agreement with the experimentally measured values for the same quantities.

By making use of these same types of methods, it is also possible to deduce, for different operational configurations of ejector nozzles, the situation concerning changes in the structure of the shock wave in the main flow. This helps us to understand the nature of the flow in the ejector nozzles being studied.

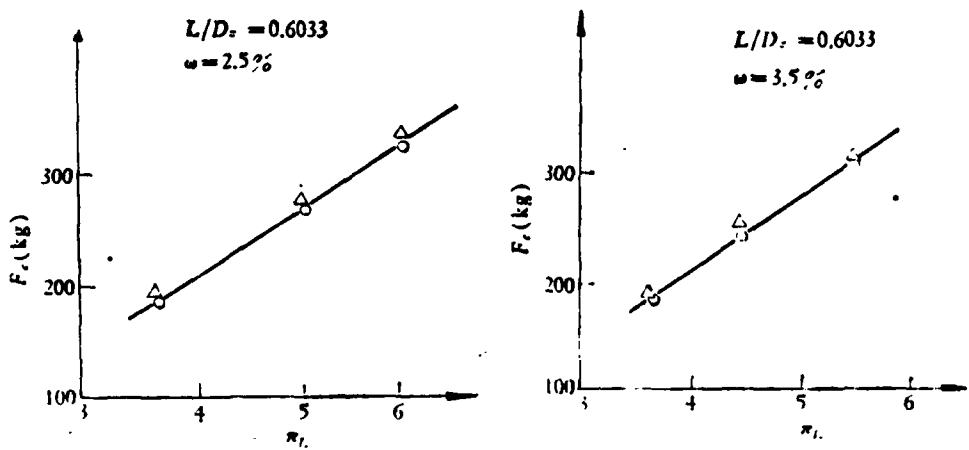


Figure 6. A comparison between the calculated values for ejector nozzle thrust and the experimentally measured values corresponding to them.

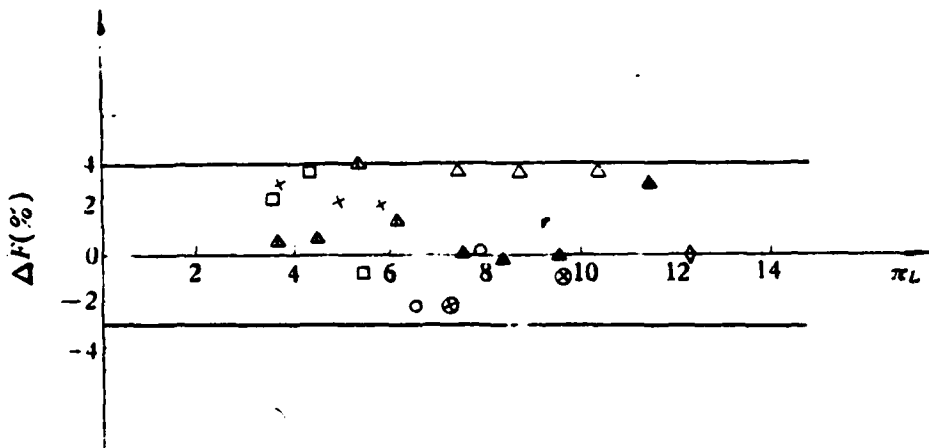


Figure 7. The errors between the calculated values for thrust in the ejector nozzles being studied and the experimentally measured values for the same quantity.

Figure 7 notes:

$L/D_e = 0.588$	$\omega = 2.59\%$	○
	$\omega = 3.5\%$	△
	$\omega = 5.0\%$	⊗
$L/D_e = 0.6033$	$\omega = 1.5\%$	▲
	$\omega = 2.5\%$	×
	$\omega = 3.5\%$	□
$L/D_e = 0.4676$	$\omega = 3.5\%$	▲

REFERENCES

- [1] В. И. Поликовский Силовые установки летательных аппаратов с воздушно-реактивными двигателями. Машиностроение 1965.
- [2] H. E. Weber, Ejector-Nozzleflow and Thrust, Tran ASME Series, D 1960, Vol. 82.
- [3] Analytical and Experimental Evaluation of Performance Prediction Methods Applicable to Exhaust Nozzle. AIAA Paper 71—719.
- [4] Element of Aerodynamics of Supersonic Flow, Ferri, A.
- [5] A Theory of the Cylindrical Ejector Supersonic Propelling Nozzle, H. Pearson JRAS 1958, No. 10.

ANALYTICAL AND EXPERIMENTAL INVESTIGATION OF SUPERSONIC EJECTOR NOZZLE

Wu Da Yang Zai-ming Zhang Rung
(*Beijing Institute of Aeronautics and Astronautics*)

Abstract

In this paper we introduce some results of test of ejector nozzle, and propose in compliance with these results a model of the flow in ejector nozzle, and so we establish an approximate method to count the thrust characteristics of it. At last we compare the results with data of test and discover that they are good in agreement.

B₁ TYPE TRANSONIC AXIAL-FLOW-COMPRESSOR FIRST STAGE ROTOR BLADE DESIGN, TEST AND APPLICATION*

Zhou Wei-guo
(Shenyang Aeroengine Company)

SUMMARY

This article describes the process of experimentation and redesign which was carried out in order to eliminate failures due to cracking of I stage B₁ type engine blades. This article is composed altogether of three sections. The first section is one which deals with the methods used to redesign the blades in question. The second section contains the results of experimentation. And the third section is an appraisal of the application of these blades.

FOREWORD

The B₁, from the time of its testproduction, both inside the factory and outside the factory, developed many instances of failures due to cracking and breaking of blades in the first stage operations of the engine. In the factory, there was one case of bending, four cases of cracking. Out in the field, there was one case of a major accident and five cases of cracking of these components, which severely influenced the safety of aircraft in the Peoples Air Force.

At that time, our analysis was this: We thought that the fifth batch of engines had common operational curves which were relatively close to the surge line and the surge margin was small. Because of this, we carried out a series of dynamic and static frequency tests. With the approval of the factory, we produced a fifth batch of thicker blades (simply called fifth batch thick blades). When dynamic and static frequency tests were made to determine these frequencies, the results of the experiments showed no obvious differences between the basic natures of the normal fifth batch blades and the thicker fifth batch blades.

*This article was read at the 2nd All China Engineering Thermophysics Technology Conference in Hangzhou in November of 1978.

In 1965, we made experimental tests for a sixth batch of engines. The first stage operational blades and the flow rectifier blades in the fourth and fifth stages saw some relatively large changes from those of the previous model. Among these changes were the facts that the operational blades in the first stage compressors (called "first flow" for short) had their arc lengths extended by 21-26 mm. The number of blades was changed from 31 to 24. The arc length of the fourth stage rectifier blades was reduced by 3-4 mm. And, the maximum thickness of the fifth stage rectifier blades was increased 0.15-0.24 mm. The flow parameters resulting from these three changes, with the exception of the five cross section of the first stage compressor blade tips β_{1K} , β_{2K} all exhibited changes. All the other parameters were the same as they were with the old form. In order to completely eliminate malfunctions due to problems with the first stage compressor components, in September of 1965, work was begun on redesigning the first stage compressors. In 1970 and in the years 1975-1976, we made more than 20 tests and these experiments are introduced below.

1. DESIGN OF THE OPERATIONAL BLADES OF THE FIRST STAGE COMPRESSORS (CONFIGURATION)

1. The arc length of the first stage compressor blades in the sixth batch of engines was lengthened by 21-26 mm over the length as it was in the fifth batch of engines. The number of blades was reduced from 31 to 24. The blade configuration parameter b/t was the same as it was with the fifth batch. And the cross sections β_{1K} , β_{2K} of the five blade tips were larger than those for the fifth batch of engines by $1^{\circ}56' - 1^{\circ}07'$. The results of these experiments were these. The temperature of the exhaust gases of the sixth batch of engines as well as their rates of fuel consumption were relatively higher than the corresponding values for the fifth batch of engines. From this fact, it can be seen that the aerodynamic performance of the fifth batch of engines was superior to that of the sixth batch of engines. When we gave consideration to the cracking malfunctions

associated with the first stage compressor blades of the fifth batch of engines, we referred to the arc length and maximum thickness of the blades of the first stage compressors of the sixth batch of engines in order to select a first stage compressor blade configuration designed on the basis of these data and the form which was designed was the I-02 blade.

This designing process was carried out in the years 1965-66. The calculations of intake flow fields which are contained in this report were done on the basis of the two-dimensional type calculation method. The blade parameters used can be seen set out in the table below.

One can see from the data in the table below that the fact that the arc length is increased and the Reynolds number is increased broadens the range of operational stability of the engine. The value \bar{C}_{max} for the sixth batch of engines is smaller than that for the fifth batch, this is an advantage for the supersonic and transonic blade performance involved. A cross section of the I blade of the sixth batch has a level straight section to it. Below the II cross section the intake has a shorter straight section to it. The blade trough has a section which gradually widens and has no throat section to it. This sort of configuration for supersonic blades does not correspond to what is normally done with this type of design and, in the design process, adjustments are needed.

2. Operational configurations of first stage blades (see Table 2).

3. The method of configuring the shape of supersonic blades (appropriate for use with values of $M = 1.15-1.40$).

(1) Draw a straight line OQ which, with the quota lines, forms β_{IK} (see Figure 1). In that figure $OQ = b(1 - 1.56r/b)$ and, in this relationship $r' = r * \sin \beta_{IK}$.

TABLE 1. A table of the parameters for the blade configurations for the fifth and sixth batches of engines

Cross section	II	I	III	IV	V	VI	VII	VIII	IX	X	XI
K	119	130.5	105.1	279.7	254.3	228.8	203.5	178.05	165.4		
b	84.6 ^a	88.55	85.66	84.47	81.05	78.76	76.7	73.61	73.02		
	116	114	110	107	103.8	101.4	98.1	94.8	93.5	(92.6)	(92)
A/Z	1.307	1.322	1.385	1.472	1.572	1.70	1.851	2.04	2.18		
β_{1K}	29°20'	31°23'	36°57'	43°45'	51°49'	62°9'	76°18'	96°6'	120°		
	12°30'	38°30'	45°	53°45'	62°	78°	97°30'	115°	(133°30')	(150°45')	—
β_{2K}	25°13'	27°14'	31°26'	35°6'	37°28'	42°55'	47°7'	51°51'	54°30'	57°22'	61°42'
	29°	33°	36°30'	39°	44°	47°15'	51°30'	54°15'	58°45'	63°	65°16'
$\bar{\epsilon}_{B\star}$	2.75	2.93	3.72	4.46	5.23	6.07	6.97	7.90	8.23		
	2.19	3.03	3.80	4.63	5.30	6.19	7.15	7.70	(8.37)	(8.70)	
$\bar{x}_c\%$	64.6	65.2	56.2	53.8	53.1	54.3	56.8	57.6			
	61	55.7	54.7	51.5	57.7	55.3	57.1	57	62	65	—
θ_1	5°45'	6°12'	7°15'	7°27'	7°36'	7°06'	7°30'	8°18'			
	3°30'	3°	4°	4°	5°15'	5°	6°15'				
θ_2	4°33'	4°33'	5°	5°42'	7°42'	9°54'	12°6'	13°54'			
	3°30'	4°45'		5°30'	7°30'	9°	11°	11°15'			
r_1	0.34	0.35	0.37	0.40	0.43	0.46	0.50	0.57	0.63		
	0.35	0.37		0.40	0.43	0.46	0.50	0.57	0.63		
r_2	0.55	0.56	0.58	0.62	0.66	0.69	0.72	0.79	0.90		
	0.40	0.45	0.50	0.54	0.55	0.60	0.85	0.90			

NOTE: The parameter values given on top are those for the fifth batch and the values given underneath are for the sixth batch of engines.

(2) If one draws a straight line QO_2 past the point Q which forms, with the rating line involved, the angle β_{2K} , then go on to the next step.

(3) Draw the tangent circle to the leading edge quota line and the line OQ . The radius of this circle is r_1 .

(4) Go through the center of the forward tangent circle O_1 . Take $b - (r_1 + r_2)$ to be the radius at QO_2 and get the point O_2 .

TABLE 2. Original data for the I-02 blade form

	0	I	II	III	IV	V	VI	VII	VIII
R	339	330.5	305.1	279.7	254.3	228.8	203.5	178.05	165.4
s	116	114.38	110.61	107.79	104.66	101.87	98.61	95.12	94.4
β_{IK}	25°13'	27°14'	31°26'	35°6'	37°28'	42°55'	47°7'	51°51'	54°30'
β_{IK}	29°20'	31°23'	36°57'	43°45'	51°49'	62°09'	76°18'	96°6'	120°
C _{cam}	2.59	2.59	3.45	4.15	4.95	5.50	6.25	6.90	7.20
X _{c%}	64.6	65.2	56.2	53.8	53.1	54.3	56.8	57.6	57
ϵ_1	2°24'	2°42'	3°39'	4°30'	5°06'	5°30'	5°45'	6°	6°6'
ϵ_2	3°42'	3°48'	4°21'	5°18'	6°54'	8°42'	8°54'	9°	9°
l_s	53	49	37	25.45	0	0	0	0	0
l_p	9.3/ 106.3	8.1/ 105.7	110	22.75	0	0	0	0	0
F _{w 1}	0.49	0.59	0.55	0.62	0.52	0.67	0.61	0.59	0.59
F _{w 2}	两直线	两直线	二直线	0.53	0.48	0.65	0.59	0.54	—
r ₁	0.34	0.35	0.37	0.40	0.43	0.46	0.50	0.57	0.63
r ₂	0.40	0.40	0.45	0.50	0.54	0.55	0.60	0.85	0.90
M _{w1}	1.36	1.33	1.23	1.18	1.09	1.04	0.98	0.91	0.87

Key: 1--back; 2--dish; 3--two straight lines; 4--two straight lines;
5--one straight line

- (5) Going through point O₂ draw a circle with radius r₂.
- (6) Join O₁O₂ and, from the value O₁ select (x_c—r₁) to get the point M.
- (7) Draw ε₁, ε₂. ε₁ is formed by drawing a line from OQ to QA₂. ε₂ is the supplementary line segment from QO₂.
- (8) Extend OQ back away from the blade and ε₂ will connect with point B₁ on one side of angle ε₂. Moreover, on OQ chose l_s = OA.
- (9) From A₁ B₁ C₁ form a triangle and select F (consult Table 3) as a secondary curve.

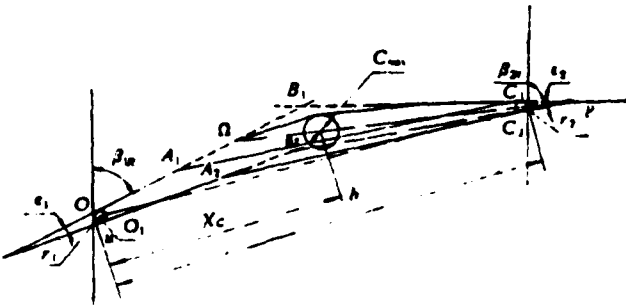


Figure 1. A schematic diagram of a supersonic blade configuration

(10) At M draw a perpendicular O_1O_2 . On this line, draw a circle C_{\max} tangent to the curve of the back of the blade.

(11) Extend ϵ_1 in the direction of the dish of the blade and select $UA_2 = l_p$.

(12) Extend ϵ_2 in the direction of the dish of the blade so that line segment PC_2 meets with UA_2 at point B_2 .

(13) Draw a secondary curve in the triangle formed from $A_2B_2C_2$.

(14) Check out the location of the point at which the thickness is largest. If the position of C_{\max} has moved beyond the designed value for it by 5%, then select new values for ϵ_1 , ϵ_2 . Begin the recalculation process from procedure (7) and continue it until one gets a satisfactory position for X_c within an acceptable tolerance (5% X_c)

4. The design of transonic blade forms (secondary curve configurations).

(1) On the basis of experience, select the position of greatest curvature of the center line X_f . At the various cross sections of the B_1 type engines $X_f = 0.5$, $F = 0.57$.

(2) On the basis of the formula $\frac{1}{g\varphi_1} = \frac{1}{g\varphi_2} \frac{\bar{F} + 1 - 2\bar{X}}{\bar{F} - 1 + 2\bar{X}}$, as well as $\theta = \varphi_1 + \varphi_2$ in combination it is possible to get values for the angles φ_1, φ_2 .

(3) $r = \rho_{ik} + \varphi_1$ (according to the angle of installation angle).

(4) From $b - r_1 - r_2, \varphi_1, \varphi_2$ draw the triangle A B C and check the table to find the center line.

(5) At points A, C make the circles r_1, r_2 and the acute angles $\varepsilon_1, \varepsilon_2$. Then solve for the tangent points A_1, A_2, C_1, C_2 between the two sides of the acute angle and the circles r_1, r_2 . After this, extend the two sides of the angle.

(6) On the centerline, make a perpendicular to AC passing through point X_c . This line intersects the centerline at point M. If one draws a diameter at point M, then it defines the circle C_{max} .

(7) One then draws a secondary curve through the triangles $A_1 B_1 C_1$ and $A_2 B_2 C_2$ which is tangent to the circle C_{max} (\bar{F} is selected).

5. Calculation of the intake area flow field cross sections in supersonic applications.

Calculations of the intake area flow field make use of a positive shock wave model. These calculations are carried out on the basis of the methods outlined in References [1] and [2] and will not be discussed in this article.

2. OPERATIONAL BLADE TESTS ON B_1 TYPE FIRST STAGE COMPRESSORS

1. These operational tests were done on two occasions altogether, once in 1970 and once in the period 1975-76. There were more than 20 individual tests. The objective of the tests in 1970 was to do research on the causes of the blade malfunctions in order to

select a design for the new I-02 type blade for use with the fifth and sixth batches of engines. The experiments done in 1975 had to do with work that had to be done before finalizing the form of the B₁ type engine (01 batch). Some supplementary experiments were also done in order to try to find the effects of installing blades with varying frequency differences on the long-term erosion of the blades and the prevention of the occurrence of vibration in order to raise the operational reliability of the blades. Besides this, tests were also run on the similar type 2C Soviet blade for purposes of comparison.

2. The contents of the tests

We made measurements, when $\bar{n} = 0.7, 0.8, 0.85, 0.90, 0.95, 1.0$, of the overall performance of the compressor and its base characteristics of performance when $\bar{n} = 1.0$ as well as of the surge margins. In order to carry out observations of the blades involved, strain panels were attached to the areas in which malfunctions often occurred (see Figure 2) and measurements were made of the frequency of the movements of the blades and of their changes in applied stress.

3. On the basis of the fact that, in the factory, there were four occurrences of cracking and one occurrence of actual breaking all of which occurred during heat test configurations and outside of the factory, there was one case of bending and five cases of cracking which occurred in high altitude situations in which large M numbers were involved, it is possible to estimate that its reduced rotation speed is $\bar{n} = 0.825—0.86$. The high altitude and temperature reduced speed of rotation is as shown in the table below, that is

configuration	heat test intake temperature		$H = 11$ kilometer	
	120°C	150°C	$M = 2$	$M = 2.1$
	0.856	0.825	0.86	0.85

From the table above, one can know that $\bar{n} = 0.85$ is the approximate critical rotational speed of malfunction and that this speed requires careful watching as well as the careful selection of the stress values involved.

4. We made measurements of the first stage performance of the compressors being tested and we made use of the rotor of the same test bed to measure \bar{n} and \bar{G} for the mechanism as a whole and these results closely followed the common operational curves for the compressors and the turbines involved.

5. New topics

On the basis of the experience of our factory with the elimination of malfunctions as that experience was acquired before 1970, the first step was to recognize the fact that blade malfunctions were generally caused by vibration fatigue and that cracking of the blades in these engines took place when $M = 0.85$ and the engine was in a heat test configuration. Moreover, such an appearance of cracking was always present when the engine involved was experiencing abnormal sonic conditions. When the period of time involved in this process was short, it was possible to see, in the blades involved, violent agitated movements. On the basis of other research materials published in China and abroad, we came to realize that this type of phenomenon was stall vibration, that is to say that in cases where the phase frequency which gives rise to the violent movements is the same as the phase frequency which is fixed by the nature of the blades involved, one gets the appearance of large amplitude vibrations and this leads rapidly to the cracking of the blades. Also, due to the fact that the violent vibrating movements of the blades causes agitation in the air, one gets the appearance of an accompanying whistling sound.

When the test operations were begun, three of the rotors were not equipped with strain plates. In the process of running tests on

Table 3.

	Configuration	I-02			Fifth Batch		
		G _B	π_K^*	η_K^*	G _B	π_K^*	η_K^*
1.0	I	64.4	1.361	0.72	63.86	1.339	0.69
	II	64.24	1.488	0.85	61.94	1.545	0.845
	III	63.66	1.52	0.853	60.12	1.534	0.818
	IV	59.91	1.556	0.82	57.66	1.556	0.782
	V	56.17	1.552	0.76	54.87	1.542	0.737
	VI	63.55	1.515	0.842			
	VII	62.77	1.537	0.848			
0.9	I	60.56	1.279	0.746	60.2	1.288	0.73
	II	59.78	1.356	0.856	58	1.378	0.85
	III	58.23	1.394	0.879	52.7	1.422	0.82
	IV	55.32	1.412	0.840			
	V	50.84	1.436	0.794			
0.85	I	58.45	1.24	0.766	58.14	1.231	0.752
	II	57.2	1.298	0.842	49.16	1.385	0.835
	III	56.24	1.325	0.863	51.69	1.378	0.863
	IV	52.16	1.364	0.843	58.30	1.358	0.880
	V	47.24	1.372	0.766	56.11	1.334	0.819
0.80	I	54.63	1.213	0.783	55.86	1.207	0.797
	II	53.84	1.247	0.845	45.25	1.384	0.827
	III	51.79	1.275	0.854	47.90	1.324	0.856
	IV	47.29	1.314	0.832	50.65	1.308	0.872
	V	41.81	1.328	0.752	54.49	1.278	0.860
0.70	I	50.48	1.154	0.792	50.5	1.149	0.776
	II	49.64	1.168	0.827	46.21	1.194	0.829
	III	46.46	1.197	0.840	40.3	1.234	0.814
	IV	42.15	1.224	0.821			
	V	37.68	1.239	0.762			

Table 3 Continued.

Sixth Batch			2 C		
G _B	π_K^*	η_K^*	G _B	π_K^*	η_K^*
65.69	1.389	0.739	65.06	1.381	0.719
55.3	1.581	0.765	64.89	1.497	1.83
57.96	1.581	0.80	64.10	1.539	0.842
60.48	1.576	0.831	59.58	1.571	0.799
63.29	1.559	0.857	62.98	1.557	0.834
			63.36	1.557	0.843
			56.6	1.569	0.753
62.07	1.295	0.748	61.19	1.282	0.724
50.20	1.454	0.78	60.52	1.367	0.852
53.38	1.446	0.816	59.14	1.384	0.847
55.62	1.442	0.847	56.86	1.415	0.838
58.71	1.421	0.874	51	1.439	0.777
59.60	1.243	0.738	58.91	1.244	0.741
46.71	1.400	0.786	58.1	1.297	0.84
50.33	1.390	0.823	57.02	1.33	0.856
53.56	1.311	0.863	53.1	1.363	0.829
56.83	1.348	0.881	48.65	1.382	0.79
57.27	1.216	0.782	56.53	1.22	0.78
43.71	1.345	0.774	54.94	1.24	0.804
47.34	1.334	0.823	53.87	1.276	0.842
51.50	1.312	0.862	49.81	1.317	0.841
54.36	1.290	0.882	45.12	1.328	0.774
51.59	1.157	0.795	51.02	1.164	0.827
38.59	1.257	0.770	49.2	1.184	0.832
41.20	1.244	0.820	46.62	1.211	0.585
45.50	1.222	0.861			
48.12	1.194	0.851			

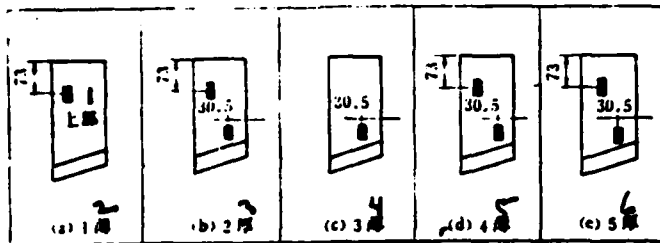


Figure 2. Strain plate positions

1--top section; 2--1 narrow; 3--2 thick; 4--3 narrow; 5--4 narrow;
6--5 thick

the blades from the fifth batch of engines, when $\bar{n} = 0.85$, one got the occurrence of an unusual whistling noise similar to the whistle of a train in the distance. Later, use was made of the strain plates in order to make observations. Stresses were found to be as high as 4500 kg/cm^3 . Because of a shortage of measurement equipment with the needed capabilities, we were capable of recognizing the existence of vibration states of the blades in the intake; however, there was no way to distinguish the different natures of these vibrations. For the results of these tests, see Table 3 and Table 4 as well as Figure 3.

3. AN EXPLANATION OF THE OVERALL RESULTS OF THE TESTS

1. For rotors in the fifth batch, except for the case in which $\bar{n} = 0.7$ from 0.75-1.0, one sees the first appearance of vibration points. The vibration threshold is very close to the operational points in this case. This is particularly true for the case in which $\bar{n} = 0.8-0.85$ which can be seen in Table 3 and Table 4.

2. The thick and thin blades in the fifth batch had no differences between them as far as their compositions were concerned. The vibration thresholds for the former were shifted somewhat to the left as compared to the vibration threshold of the latter. However, the difference was not obvious.

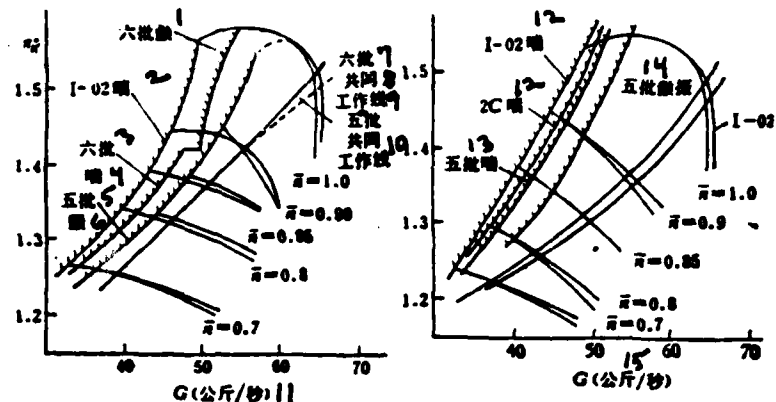


Figure 3. Performance of B_1 type first stage compressors
 1--sixth batch vibration; 2--surge; 3--sixth batch; 4--surge; 5--
 fifth batch; 6--vibration; 7--sixth batch; 8--common operational
 curve; 9--fifth batch; 10--common operational curve; 11--kg/sec;
 12--surge; 13--fifth batch surge; 14--fifth batch vibration;
 15--kg/sec

TABLE 4

	I-02			Fifth batch			Sixth batch			2C		
	\bar{n}	G_B	π_K^B	\bar{n}	G_B	π_K^B	\bar{n}	G_B	π_K^B	\bar{n}	G_B	π_K^B
Surge vibration threshold	1.08	49.09	1.548	1.0F	56.64	1.552	1.0F	52.13	1.57	1.0F	50.5	1.52
	0.95	44.26	1.446	0.95F	53.76	1.494	0.95F	47.62	1.576	1.0S	49.7	1.52
	0.85S	41.33	1.393	0.90F	50.75	1.447	0.9F	47.12	1.459	0.90S	46.1LF	1.438
	0.8S	38.19	1.339	0.85F	45.41	1.393	0.9S	46.65	1.459	0.90S	45.5LGF	1.438
	0.7S	32.39	1.25	0.80F	41.64	1.348	0.85S	43.4	1.40	0.80S	39.4LF	1.33
				0.70S	32.51	1.256	0.80S	40.42	1.346	0.80S	39LGF	1.33
振动--F 喷射--S 小频差 LF 大频差 LGF							0.70S	33.6	1.239	0.7S	33.8LF 34LGF	1.246

1--vibration; 2--surge; 3--small frequency difference; 4--large frequency difference

3. Concerning the surge threshold of the sixth batch, when $\bar{n} = 0.9-1.0$, first there is vibration and then surge. The amount of flow jumps. At this time, $\Delta G = 1.27 \text{ kg/sec}$. At other speeds of rotation, there is surge but no vibration. The boundary is located between I-02 and the fifth batch.

4. Concerning the boundaries which pertain to the I-02 blades, there is a distinction that must be made. If one is considering the

case in which there is a large frequency difference distribution, then there is no vibration boundary. In the case in which there is a small frequency distribution, that is, when $\bar{n} = 0.9-1.0$, vibration does occur. In the tests that were done on I-02 blades in 1970, there was no vibration.

5. Concerning 2C blades, they are basically the same as the I-02 blades; however, they do exhibit vibration. From the tests which were described above, it can be seen that the values which are selected for the blade density, aspect ratio, chord length and C_{max} as well as the selection of varying angles of attack and lag angle do not just influence the amounts of flow and the efficiency, but they also influence the vibration threshold of the blades involved. The application of varying frequency differences has obvious effects on the continuation or elimination of vibration.

CONCLUSIONS

1. Thin blades from the fifth batch can easily exhibit intake vibration when $\bar{n} = 0.8-0.85$. The thick blades from the fifth batch, when $\bar{n} = 0.8-0.85$, have a vibration range which is somewhat improved over that of the thin blades. 2C blades exhibit vibration when $\bar{n} = 0.95-1.0$, and the stress on them is 2960 kg/cm^2 .

As far as a comparison of the three types of moving blades is concerned, the I-02 blade is capable of the safest operation.

2. Concerning the use of equipment having large frequency difference distributions, in order to cause an improvement in the vibration of the blades being considered, the use of such a large frequency difference causes the boundary line involved to move to the left. The 2C and I-02 blades, because of the small frequency distributions installed with them, still do exhibit vibration. However, if they are employed with large frequency differences, then it is possible to eliminate vibration. The author knows this method to be effective.

3. Looking from the point of view of performance, in terms of the amount of flow and the pressure ratios involved, the 2C blades are the larger and the I-02 blades are in the middle. In terms of efficiency, the I-02 blades are the highest, the 2C blades are in the middle and the fifth batch blades are slightly lower than the 2C blades.

4. Experimental error as reflected in a comparison between the 1970 and 1975 data.

(1) Error in amounts of flow $\bar{n} = 1.0$ (when the throttle is all the way open, for example)

$$I-02 \Delta G = 0.5 \text{ kg/sec}$$

$$\text{fifth batch } \Delta G = 0.24 \text{ kg/sec}$$

$$2C \Delta G = 0.1-0.33 \text{ kg/sec}$$

(2) Concerning the pressure ratio error, when $\bar{n} = 1.0$ is taken as the example, the 1975 data is slightly lower than the data for 1970.

(3) As far as errors in efficiency are concerned, the values of η_k for the three types of rotors in the 1975 tests are all lower than the corresponding values from the 1970 tests. This is primarily determined by measurement errors in \bar{G}_B , π_k^* and N (power).

Considering the errors described above as a whole, the tests which have been spoken of in this article had to do with the determination of the displacements and direction of movement of the surge and vibration boundaries under differing conditions; therefore, these errors can have no substantial effects on the findings.

References

- [1] G. R. Miller and M. J. Hartmann: Experimental shock configurations and shock losses in transonic compressor rotor at design speed, NACA RM E58A14B, 1958.
- [2] F. C. Schwenk, G. W. Lewis, Jr. M. Hartmann: A preliminary analysis of the magnitude of shock losses in transonic compressor, NACA RM E57A30.
- [3] В. А. Андреев: Расчет и построение контров самолета на плазе, Оборониздат, 1960.

B₁ TYPE TRANSONIC AXIAL-FLOW-COMPRESSOR 1ST STAGE ROTOR BLADE DESIGN, TEST AND APPLICATION

Zhou Wei-guo

(Shenyang Aeroengine Company)

Abstract

This paper describes the design modification of the 1st stage rotor blade to relieve crack development and presents test result of the modified blades.

END
DATE
FILMED
10-81
DTIC